Rational design of selective bispecific EPO-R/CD131 agonists

Kailyn E. Doiron[1,2,3], Jeffrey C. Way[1,2], Pamela A. Silver[1,2]*

1. Department of Systems Biology, Harvard Medical School, Boston, Massachusetts, 02115, USA
2. Wyss Institute for Biologically Inspired Engineering, Harvard University, Boston, Massachusetts 02115, USA
3. Harvard Systems, Synthetic and Quantitative Biology PhD Program, Harvard University, Cambridge, Massachusetts 02138

Corresponding author: Jeffrey C. Way
jeffrey_way@hms.harvard.edu

Abstract

Erythropoietin (EPO) suppresses apoptosis and promotes survival by signaling through EPO-R/EPO-R on hematopoietic progenitors or EPO-R/CD131 on non-hematopoietic cells. However, EPO signaling through EPO-R/CD131 is controversial and there is no solved structure of a complex. Here, we constructed a structural model of EPO-R/CD131 and designed several anti-EPO-R, anti-CD131 bispecific proteins that selectively activate EPO-R/CD131. Treatment with these fusion proteins is sufficient to activate STAT5 phosphorylation downstream of EPO-R/CD131 without engaging EPO-R/EPO-R. We demonstrated that proteins with a tandem scFv or bispecific antibody format activate EPO-R/CD131, in contrast to an equimolar mixture of the individual scFvs. Finally, we explored the effect of modifications to binding domain arrangement and linker length and found results consistent with our structural model of an EPO-R/CD131 complex. These findings highlight the utility of bispecific scaffolds in the development of cytokine receptor agonists and provide a foundation for the study of EPO-R/CD131 biology and future clinical development.

Graphical Abstract

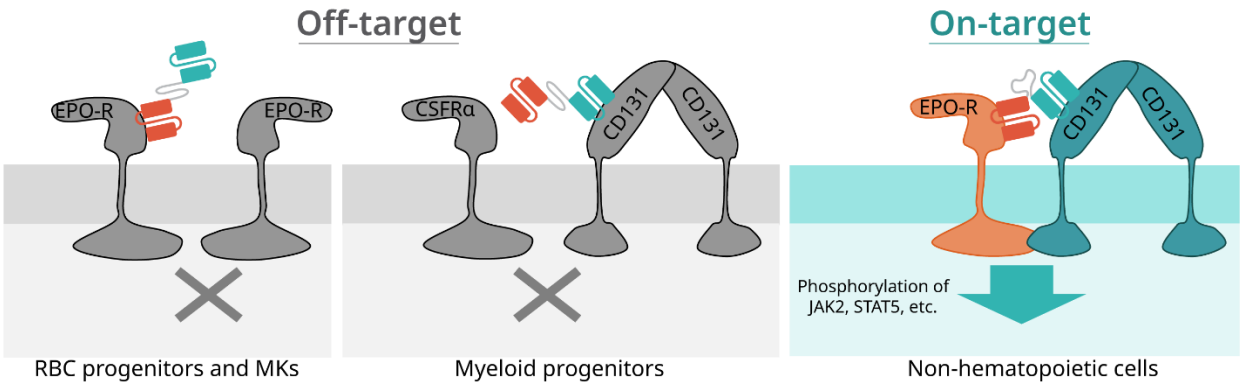

Keywords

scFv

Erythropoietin

Cytokine

Rational Design

Neuroprotection

STAT5

Introduction

Erythropoietin (EPO) is a cytokine that is essential for red blood cell (RBC) maturation. EPO promotes erythropoiesis by suppressing apoptosis in a subset of erythroid progenitors, enabling their survival and subsequent differentiation (Watowich, 2011). EPO signaling in these cells is well-characterized and begins through binding of EPO to the homodimeric EPO receptor (EPO-R/EPO-R) (Broudy *et al.*, 1991; Philo *et al.*, 1996; Watowich, 1999). Ligand binding induces structural changes in the cytoplasmic domains of EPO-R, triggering transactivation of JAK2 and then STAT5 (Witthuhn *et al.*, 1993; Chin *et al.*, 1996; Klingmüller *et al.*, 1996). Once STAT5 is phosphorylated by JAK2, it translocates to the

nucleus where it activates expression of genes necessary for the survival, proliferation and differentiation of erythroid cells, including the anti-apoptotic proteins Bcl-2, Bcl-XL (Wojchowski *et al.*, 1999; Watowich, 2011). Due to its ability to promote erythropoiesis, EPO and its derivatives (e.g. Epoetin alfa, Darbepoetin alfa) are FDA-approved drugs for the treatment of anemia resulting from chronic kidney disease or chemotherapy.

EPO signaling also drives activated platelet generation, expression of pro-thrombotic proteins, protection of non-hematopoietic cells against hypoxic stress, and nitric oxide production by the vascular epithelium (Lippi *et al.*, 2010; Sautina *et al.*, 2010; Lee *et al.*, 2020; Sergio and Rolando, 2022). To explain these diverse responses, we have proposed previously that EPO mediates the body's response to hemorrhage, simultaneously protecting tissues against reduced oxygen and promoting cessation of bleeding and the generation of new RBCs (Burrill *et al.*, 2016; Lee *et al.*, 2021). The protection against stress is not limited to hypoxia; EPO reduces cell death responses to a variety of stimuli. Due to its anti-apoptotic properties, there has been interest in using EPO in disease states such as traumatic brain injury, myocardial infarction, and neurodegenerative diseases such as ALS (Ghezzi and Brines, 2004; Grunfeld *et al.*, 2007; Gan *et al.*, 2012; Patel *et al.*, 2012; Hernández *et al.*, 2017; Robinson *et al.*, 2018). However, the dose of EPO needed to activate protective signaling (~1-20 nM) is generally higher than the dose necessary for its effects on erythroid and megakaryocytic cells (100-200 pM) (Anagnostou *et al.*, 1990; Masuda *et al.*, 1993; Brines and Cerami, 2008). At these doses, the likelihood of off-tissue EPO-R homodimer-driven effects, such as RBC and platelet generation, increases (Brines and Cerami, 2008).

Tissue-protective signaling by EPO is thought to be mediated, at least in part, by a heterodimer of EPO-R and CD131; however, the details of this signaling mode are unclear and controversial (Brines *et al.*, 2004; Cheung Tung Shing *et al.*, 2018). CD131, the common beta receptor (βc), is the beta subunit of the GM-CSF, IL-3, and IL-5 receptors and is crucial for the differentiation of a diverse set of myeloid cell types (Scott and Begley, 1999). There is substantial evidence that EPO-R and CD131 interact. Jubinsky et al. (Jubinsky *et al.*, 1997)

first demonstrated that CD131 functionally associates with EPO-R through co-immunoprecipitation experiments, and Hanazono et al. (Hanazono *et al.*, 1995) observed phosphorylation of CD131 in response to EPO. Moreover, Sautina et al. (Sautina *et al.*, 2010) found that co-immunoprecipitation of EPO-R with anti-CD131 was enhanced by EPO, but they also found that the VEGF receptor was also co-immunoprecipitated with EPO-R and anti-CD131. However, Cheung Tung Shing et al. (Cheung Tung Shing *et al.*, 2018) failed to find evidence of an interaction between the extracellular domains of EPO-R and CD131 in the presence of EPO. In sum, the structure of an EPO-R/CD131 complex and how these proteins interact to induce downstream signaling is still controversial.

To selectively activate EPO-R/CD131 many groups have developed EPO derivatives that putatively reduce or eliminate activation of homodimeric EPO-R, such as carbamylated EPO (cEPO) (Leist *et al.*, 2004), EPO mutants with lower affinity for EPO-R (Leist *et al.*, 2004; Gan *et al.*, 2012; Lee *et al.*, 2021), smaller peptide derivatives of EPO (Brines *et al.*, 2008; Pankratova *et al.*, 2012; Ercan *et al.*, 2018; Cho *et al.*, 2022) or small EPO-mimetic peptides (Wrighton *et al.*, 1996; He *et al.*, 2019). The most studied EPO alternative is carbamylated EPO, in which all amino groups on the ten lysines have a carbamyl modification. cEPO has been proposed as a neuroprotective therapeutic that does not produce red blood cells or platelets and is claimed to signal only through EPO-R/CD131 and not through EPO-R homodimers (Leist *et al.*, 2004). However, to the best of our knowledge, the quantitative effect of carbamylation on EPO's binding to EPO receptor or CD131 has not been characterized (e.g. by surface plasmon resonance), nor has its activity been rationalized in terms of solved structures of CD131 or EPO and EPO-R.

Additionally, cEPO has the same plasma half-life as EPO itself – about eight hours (Macdougall *et al.*, 1989). In the treatment of anemia, EPO can be used intermittently because treatment produces a burst of erythroid progenitor activity that produces red blood cells lasting 100 days. However, neuroprotection by EPO signaling may require continuous exposure, which may require genetically fusing a hormone to a module that extends half-life such as albumin or the Fc region of an antibody. Rational design of such

92 an engineered protein would require a structural understanding of how EPO, EPO-R and
93 CD131 interact. The focus of the present work is to explore the structure of the EPO-
94 R/CD131 signaling complex at a level sufficient to construct engineerable fusion proteins
95 that will activate EPO-R/CD131 selectively over EPO-R/EPO-R.

96

97 ## Results

98 ### Rational design of tandem scFv proteins for selective activation of EPO-R/CD131

99 We aimed to develop selective agonists of EPO-R/CD131 that do not activate EPO-
100 R/EPO-R. Given the mechanisms of complex formation of the GM-CSF receptor (Carr *et al.*,
101 2001; Hansen *et al.*, 2008; Caveney *et al.*, 2024) and EPO-R/EPO-R (Watowich *et al.*, 1994,
102 1999; Syed *et al.*, 1998), we hypothesized that binding EPO-R and CD131 using a bispecific
103 molecule would be sufficient for pathway activation through induced proximity. To
104 explore how binding flexibility and orientation may affect receptor activation, we designed
105 three fusion proteins with distinct structural configurations. Each protein is bispecific and
106 designed to bind both EPO-R and CD131. We first generated a tandem scFv, whereby two
107 scFvs are joined by a linker to generate a single-chain bispecific binder. This protein
108 (denoted as TscFv) consists of two previously reported high-affinity scFvs (Borges *et al.*,
109 2008; Moraga *et al.*, 2015; Panousis *et al.*, 2016) connected with a flexible glycine, serine,
110 and glutamic acid linker **(Figure 1A)**. We then fused either the entire TscFv or the
111 individual scFvs to the fragment crystallizable domain (Fc) of mouse IgG2a (**Figure 1A**)
112 since Fc fusion can improve the stability, manufacturability, and serum half-life profiles of
113 biologics. The first Fc fusion protein is a bispecific antibody with each scFv fused to one
114 half of Fc (denoted as BsAb), and the second Fc fusion consists of the entire TscFv linked to
115 one half of Fc (denoted as TscFv-Fc) **(Figure 1A).** To ensure both halves of the bispecific Fc
116 fusion proteins are present, we used a previously published heterodimeric Fc variant that
117 favors heterodimer formation through electrostatic steering (Wang *et al.*, 2019). This
118 improves the likelihood of retaining both halves of Fc after purification. The desired

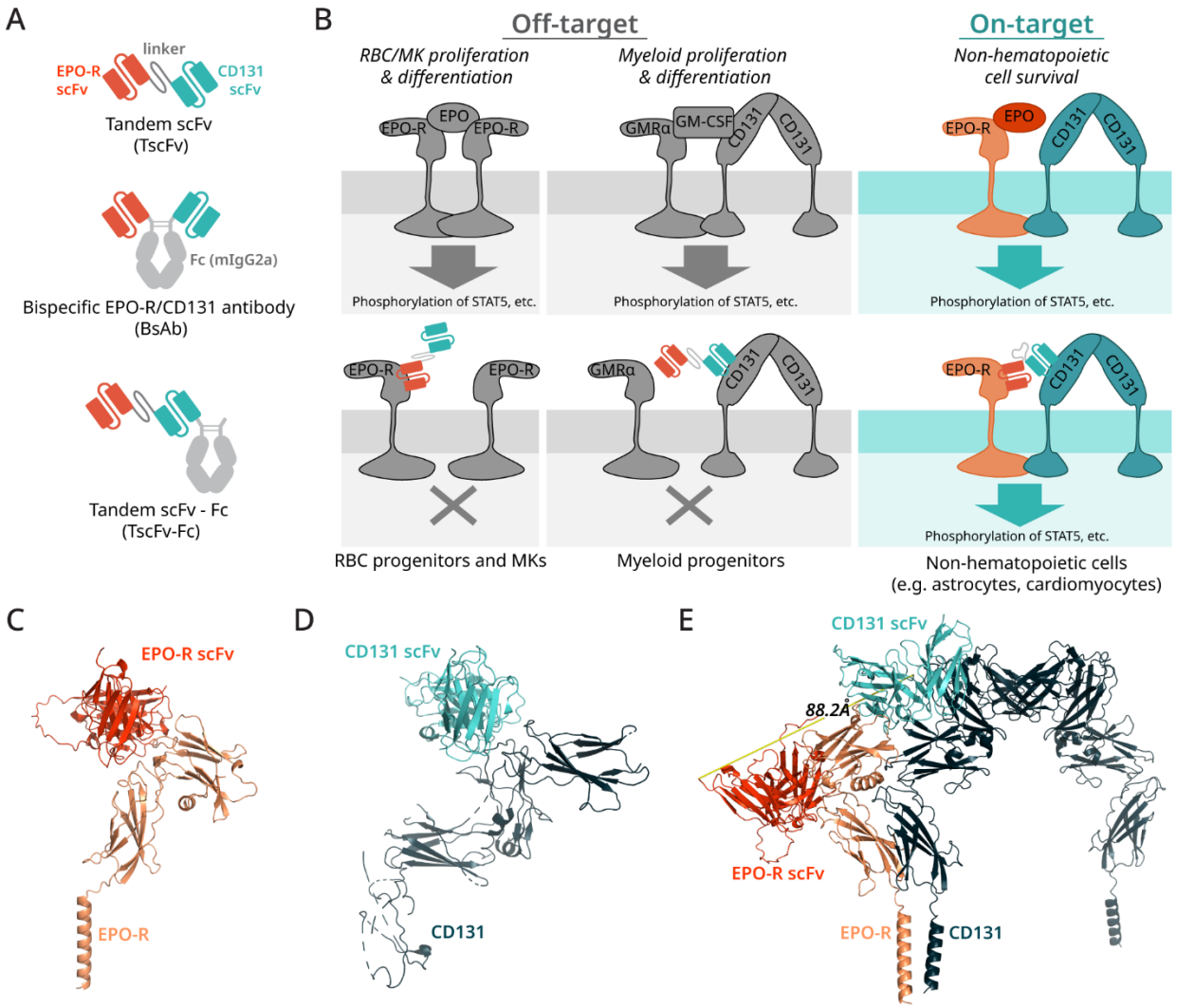

Figure 1. Design rationale for tandem scFvs that selectively target EPO-R/CD131.

A. Schematic of the three bispecific fusion proteins explored in this work. Each consists of a previously published EPO-R binding scFv (Borges *et al.*, 2008; Moraga *et al.*, 2015) and a previously published CD131 binding scFv (Panousis *et al.*, 2016). The first protein (TscFv) is a tandem scFv whereby the EPO-R scFv and the CD131 scFv are joined by a long linker to make a single chain, bispecific binder. The other two proteins consist of the binding moieties fused to the fragment crystallizable (Fc) region of mouse IgG2a. Fusion to Fc is expected to enhance half-life due to an increase in size (and therefore a decrease in the rate of renal clearance) and FcRn-mediated recycling (Kontermann, 2011). One Fc fusion consists of the scFvs individually fused to the N terminus of Fc, forming a bispecific antibody (BsAb), and the other consists of the entire TscFv fused to one half of Fc (TscFv-Fc). **B.** Schematic of endogenous signaling through EPO-R and CD131 compared to the desired pathway activation by our fusion proteins. EPO naturally signals through either homodimeric EPO-R (which mediates RBC and platelet generation) or EPO-R/CD131. Our fusion proteins are designed to

eliminate the activation of EPO-R homodimers to mimic EPO-induced activation of EPO-R/CD131 with enhanced selectivity. **C.** Solved structure of the EPO-R scFv bound to EPO-R (Moraga *et al.*, 2015) **D.** Solved structure of the CD131 scFv bound to one monomer of CD131 (Panousis *et al.*, 2016)**. E.** Alphafold 3 (Abramson *et al.*, 2024) and pyMOL prediction of the potential structure of the tandem scFv in complex with EPO-R/CD131. We used Alphafold 3 to predict the interaction of each scFv with hEPO-R and $(CD131)_2$. Then we aligned both structures using the common elements (i.e. hEPO-R and $(CD131)_2$. The resulting structure is a possible prediction of how EPO-R and CD131 may interact. In this model the C-terminus of the EPO-R scFv is 88 angstroms away from the N-terminus of the CD131 scFv. We used this model to design the linker to our tandem scFv, ensuring it could span that distance.

signaling of these three molecules is depicted in contrast to endogenous signaling of EPO in **Figure 1B**.

Since there is no structural information for a hypothetical EPO-R/CD131 complex, we used available structural data of the scFvs binding to their respective receptors (**Figure 1C, 1D**) and AlphaFold (Abramson *et al.*, 2024) to model the potential interaction of EPO-R/CD131 and TscFv **(Figure 1E)**. Specifically, we first generated one model of anti-EPO-R/EPO-R/$(CD131)_2$, and a separate model of anti-CD131/EPO-R/$(CD131)_2$ using AlphaFold. We included two copies of CD131 since it naturally forms a non-signaling dimer in which the two transmembrane segments are separated by 90-140 Å (Carr *et al.*, 2001). In the two predicted complexes, EPO-R and $(CD131)_2$ have a similar geometry as in these structures. We aligned the complexes using PyMol so that the EPO-R and $(CD131)_2$ molecules in each model were maximally aligned, and then we inferred the relationship of the anti-EPO-R and anti-CD131 scFvs as a hypothetical geometry to be tested. Using this structure, we measured an approximate distance the scFvs could be in the fully formed complex, which informed our linker design. In the structural model, the C terminus of the EPO-R scFv is positioned 88.2 Å from the N terminus of the CD131 scFv **(Figure 1E).** Assuming an average amino acid contour length of 4 Å, (Ainavarapu *et al.*, 2006) this distance could be covered by a ≥22 amino acid (aa) linker. Therefore, our first TscFv design connects the EPO-R and CD131 scFvs with a 23 aa linker consisting of glycine, serine and glutamic acid

161 to allow unimpeded long-range movement of each scFv and to increase overall solubility.
162 The spacing of the scFvs in BsAb might also be sufficient to allow simultaneous binding
163 since the distance between the Fabs of wildtype mouse IgG2a, is 117 ± 37 Å (Sosnick *et al.*,
164 1992).

165 The proposed model has features that are consistent with past observations about
166 a putative EPO-R/CD131 interaction. In the structural model, EPO-R associates with CD131
167 along a face away from the EPO binding site, such that if EPO were bound to EPO-R in this
168 complex, EPO would not contact CD131. Such an interaction might nonetheless be
169 promoted by EPO if we envision that unliganded EPO-R exists primarily in a self-inhibited
170 dimeric state implied by the crystal structure (Livnah *et al.*, 1999) in equilibrium with an
171 unliganded monomer. In the unliganded dimer, EPO-R interacts with itself by the same
172 surface that binds to EPO, and the geometry of this interaction would force the EPO-R
173 dimer to lie flat against the cell membrane. Additionally, EPO would bind to the
174 unliganded monomer and prevent re-formation of the inactive dimer so the EPO/EPO-R
175 complex could then interact with CD131. This kinetic model would explain how high
176 concentrations of EPO variants with a mutation in the "weak face" surface that interacts
177 with the second EPO-R could still signal through EPO-R and CD131. This structural and
178 kinetic model is further explored in the Supplementary Information.

179 We first assessed whether fusion of the scFvs to each other or to Fc would hinder
180 their binding. We expressed and purified each protein and verified the presence of
181 heterodimers in the case of the Fc fusions **(Figure S1E and S1F)**. Then, we determined
182 whether the constructs bind EPO-R and CD131 by elisa. TscFv, TscFv-Fc and BsAB all bound
183 both receptors (**Figure 2A, 2B**), though with differing apparent affinities. TscFv exhibited
184 the strongest apparent affinity for both EPO-R and CD131 and EC_{50}s for both receptors are
185 similar **(Figure 2A, 2B)**. These results demonstrate TscFv folds properly, and the tandem
186 scFv format is flexible enough to allow proper receptor binding.

187 In contrast, both Fc fusion constructs (BsAb and TscFv-Fc) had at least an order of
188 magnitude lower apparent binding affinity for either receptor when compared to TscFv.

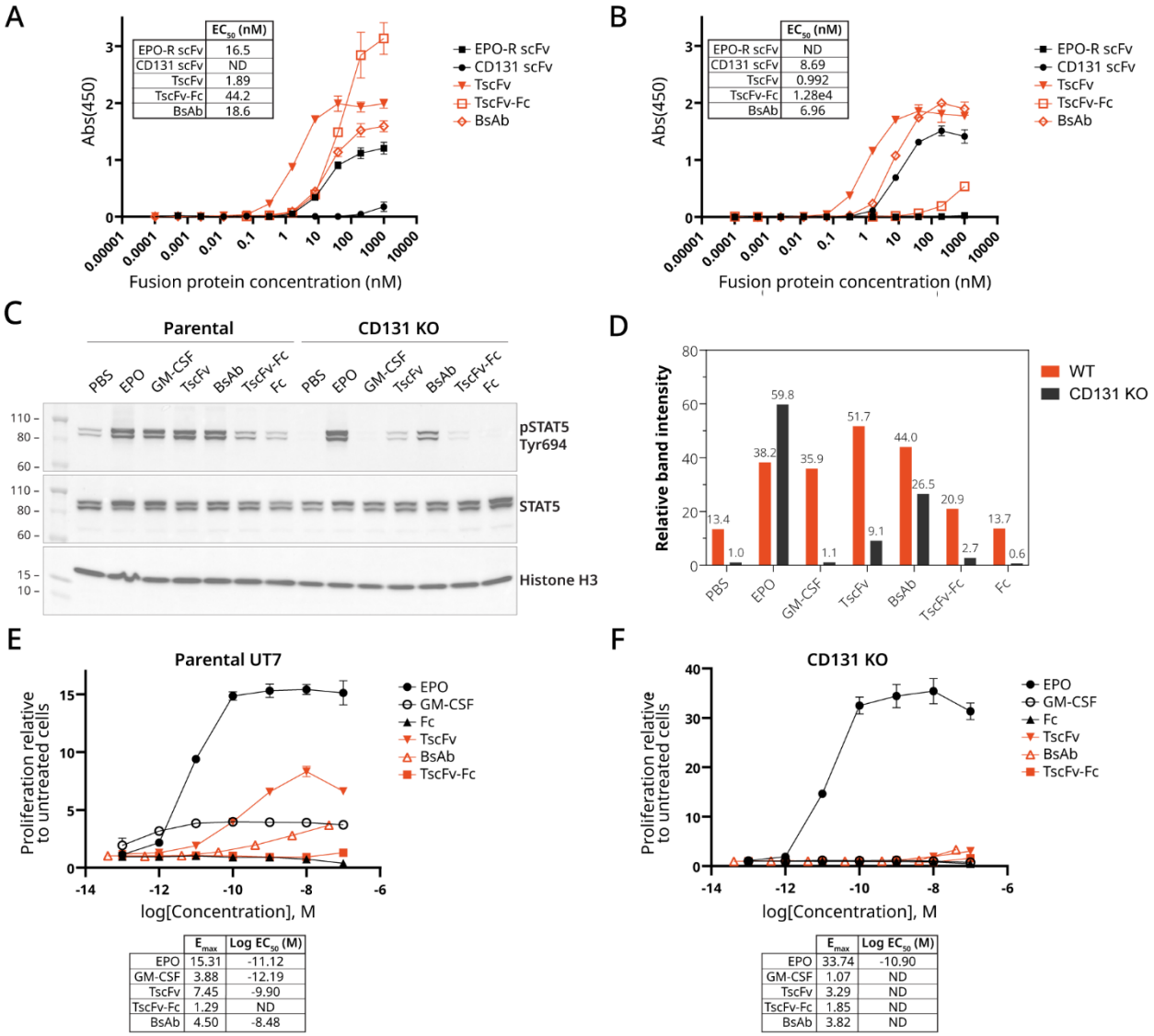

	EC_{50} (nM)
EPO-R scFv	16.5
CD131 scFv	ND
TscFv	1.89
TscFv-Fc	44.2
BsAb	18.6

	EC_{50} (nM)
EPO-R scFv	ND
CD131 scFv	8.69
TscFv	0.992
TscFv-Fc	1.28e4
BsAb	6.96

	E_{max}	Log EC_{50} (M)
EPO	15.31	-11.12
GM-CSF	3.88	-12.19
TscFv	7.45	-9.90
TscFv-Fc	1.29	ND
BsAb	4.50	-8.48

	E_{max}	Log EC_{50} (M)
EPO	33.74	-10.90
GM-CSF	1.07	ND
TscFv	3.29	ND
TscFv-Fc	1.85	ND
BsAb	3.82	ND

Figure 2. Tandem scFv and BsAb bind EPO-R and CD131 and activate downstream CD131-dependent STAT5 phosphorylation and proliferation in UT-7-ES1. A-B. Elisa of each of the bispecific proteins binding to EPO-R or CD131. Recombinant **A.** EPO-R or **B.** CD131 were used to coat elisa plates and relative binding of each protein to both receptors was determined by elisa. Elisa data are reported as mean A_{450} ± SD of three replicates. EC_{50} values were calculated using GraphPad Prism. **C.** All fusion proteins activated the phosphorylation of STAT5 at Tyr694. UT-7 EPO S1 (UT-7-ES1) is a cell line that is dependent on signaling through EPO-R/EPO-R, EPO-R/CD131, or GMCSFRα/CD131 to survive. Parental UT-7-ES1 or a UT-7-ES1 clonal CD131 KO line were FBS starved overnight, treated with 100nM proteins for 15 min, and lysed in the presence of protease and phosphatase inhibitors. Proteins were run by SDS-PAGE and visualized by western blot with the designated antibodies. **D.** Quantification of the density of sample bands in **C** relative to PBS treated sample from the CD131 KO line. **E.** TscFv and BsAb support growth of parental UT-7-ES1. UT-7-ES1 were cytokine

201 starved overnight, treated with the designated proteins and viability was measured 72 hrs later. **F.** TscFv and
202 BsAb do not support growth of UT-7-ES1 with CD131 KO. A clonal CD131 KO UT-7-ES1 line was cytokine starved
203 overnight, treated with the designated proteins and viability was measured 72 hrs later. Proliferation data are
204 reported as proliferation relative to untreated cells and are represented by mean luminescence ± SD of three
205 replicates. EC_{50} values were calculated using GraphPad Prism.

206

207 TscFv-Fc and BsAb exhibited similar binding to EPO-R (**Figure 2A**) with EC_{50}s of 44.2 nM
208 and 18.6 nM respectively. However, TscFv-Fc has severely impaired binding (12,800 nM) to
209 CD131 compared to the other proteins (**Figure 2B**), suggesting steric hindrance from the
210 Fc or the lack of flexibility of that scFv due to its fusion to the C terminus to Fc. Overall, our
211 rationally designed proteins are readily expressed and purified and bind both EPO-R and
212 CD131 as expected.

213

214 **EPO-R/CD131 tandem scFv and BsAb induce CD131-dependent STAT5 signaling and**
215 **proliferation in UT-7-ES1 cells**

216 To determine if our proteins could activate EPO-R signaling, we first assessed their
217 ability to support the growth of an EPO-responsive cell line, UT-7 EPO S1 (herein referred
218 to as UT-7-ES1). UT-7-ES1 (Shimomura *et al.*, 1992; Komatsu *et al.*, 1993) expresses both
219 EPO-R and CD131 and is dependent on either EPO or GM-CSF for growth. Consequently,
220 signaling from EPO-R/EPO-R, EPO-R/CD131, or GM-CSFRα/CD131 could be sufficient to
221 support proliferation. Western blotting to detect phosphorylated STAT5 (Tyr694) revealed
222 faint bands at the correct molecular weight for STAT5A and STAT5B in the unstimulated
223 cell line, indicating some level of basal STAT5 activation in UT-7-ES1.

224 As expected, the natural cytokines that support cell proliferation, EPO or GM-CSF,
225 induced approximately 3-fold higher STAT5 phosphorylation than both negative controls
226 (PBS and Fc) (**Figure 2C, 2D**). Both TscFv and BsAb also activated STAT5 phosphorylation,
227 inducing 3 to 4-fold higher phosphorylation of STAT5 when compared to the PBS or Fc

228 treated samples respectively (**Figure 2C, 2D**). TscFv-Fc elicited less STAT5 phosphorylation
229 than TscFv and BsAb (**Figure 2C, 2D**), possibly due to its impaired CD131 binding at this
230 concentration compared to TscFv and BsAb (**Figure 2B**). In sum, EPO, GM-CSF, TscFv, and
231 BsAb all induced STAT5 phosphorylation in the parental UT-7-ES1 cell line.

232 Since STAT5 phosphorylation can be activated through either EPO-R/EPO-R or EPO-
233 R/CD131, we assessed whether CD131 expression was required. We used standard
234 CRISPR-Cas9 gene-editing to generate a clonal UT-7-ES1 CD131 knockout (Clone C; **Figure**
235 **S2**). This knockout line has a 25-bp deletion in exon 4 (**Figure S2D**), which is in the first
236 domain of CD131, the main extracellular domain that interacts with GM-CSF. A western
237 blot using an anti-CD131 antibody against parental UT-7-ES1 revealed three bands (**Figure**
238 **S2A**), and the two high-molecular weight bands are knocked out in the UT-7-ES1 Clone C
239 cell line (**Figure S2B**). In this knockout line, CD131 KO eliminated the basal STAT5
240 phosphorylation of untreated samples that we observed in parental UT-7-ES1 **(Figure 2C,**
241 **2D)**.

242 As expected, treatment with GM-CSF no longer induced STAT5 phosphorylation in
243 UT-7-ES1 clone C (**Figure 2C, 2D)**, verifying functional knockout of CD131. Also as
244 expected, STAT5 phosphorylation induced by EPO is not reduced in the CD131 KO cell line
245 since signaling can still occur through homodimeric EPO-R (**Figure 2C, 2D)**. Each
246 engineered bispecific construct induced some level of STAT5 phosphorylation in this line
247 despite the lack of functional CD131. However, STAT5 phosphorylation was markedly
248 reduced, and all three bispecific constructs induced less STAT5 phosphorylation than EPO
249 **(Figure 2C, 2D)**. The weak remaining induction of STAT5 phosphorylation by our proteins
250 could be due to binding of the anti-CD131 scFv element to a fragment of CD131 in the
251 Clone C cell line **(Figure S2B, S2D).**

252 Next, we determined whether the stimulation provided by our fusion proteins was
253 able to support proliferation of UT-7-ES1. As expected, cytokine-starved parental UT-7-ES1
254 cells showed dose-dependent survival after treatment with EPO or GM-CSF **(Figure 2E).**
255 Parental UT-7-ES1 cells treated with TscFv or BsAb also induced dose-dependent survival

256 of UT-7-ES1, although the potency and efficacy was less than EPO **(Figure 2E).** These data
257 demonstrate that the natural ligands, EPO and GM-CSF, and two of our engineered
258 proteins, TscFv and BsAb, are able to support dose-dependent proliferation of UT-7-ES1.

259 In the UT-7-ES1 CD131 KO line, EPO, but not GM-CSF, supported proliferation
260 **(Figure 2F, Figure S2)**, verifying the functional knockout of CD131. However, in contrast to
261 the parental UT-7-ES1 cell line, CD131 KO cells treated with TscFv and BsAb did not
262 proliferate at any dose tested **(Figure 2F**). Our final engineered protein, TscFv-Fc, did not
263 support proliferation of either Parental or CD131 KO UT-7-ES1 **(Figure 2E, 2F)** which is
264 consistent with the STAT5 phosphorylation (**Figure 2C, 2D**) and CD131 binding (**Figure 2B**)
265 data. In sum, TscFV and BsAb induce CD131-dependent STAT5 phosphorylation and
266 proliferation in UT-7-ES1, similarly to EPO and GM-CSF.

267

268 **EPO-R/CD131 tandem scFv and BsAb selectively activate EPO-R/CD131 but not EPO-**
269 **R/EPO-R**

270 To further investigate the pathway selectivity of the tandem scFv proteins, we next
271 compared treatment responses in engineered human embryonic kidney (HEK293T) cell
272 lines overexpressing EPO-R, CD131 or both EPO-R and CD131 **(Figure 3A, Figure S3).**
273 Parental HEK293T do not express either EPO-R or CD131. We transduced HEK293T cells
274 with lentiviral expression constructs encoding EPO-R, CD131 or both receptors to yield
275 pooled cell lines with stable receptor expression. Each cell line was transduced
276 independently, and they are not lineally related (i.e., the cell line expressing both EPO-R
277 and CD131 is not a derivative of either the EPO-R or CD131 only line). Both receptors were
278 FLAG-tagged to verify expression of each receptor (**Figure 3B, 3C, Fig S3**). The cell line
279 expressing EPO-R can only signal through homodimeric EPO-R, while the line that
280 expresses both EPO-R and CD131 can signal through both homodimeric EPO-R and EPO-
281 R/CD131 signaling. Comparing the treatment responses of these two cell lines enables the
282 determination of selectivity by showing whether CD131 is required for activation

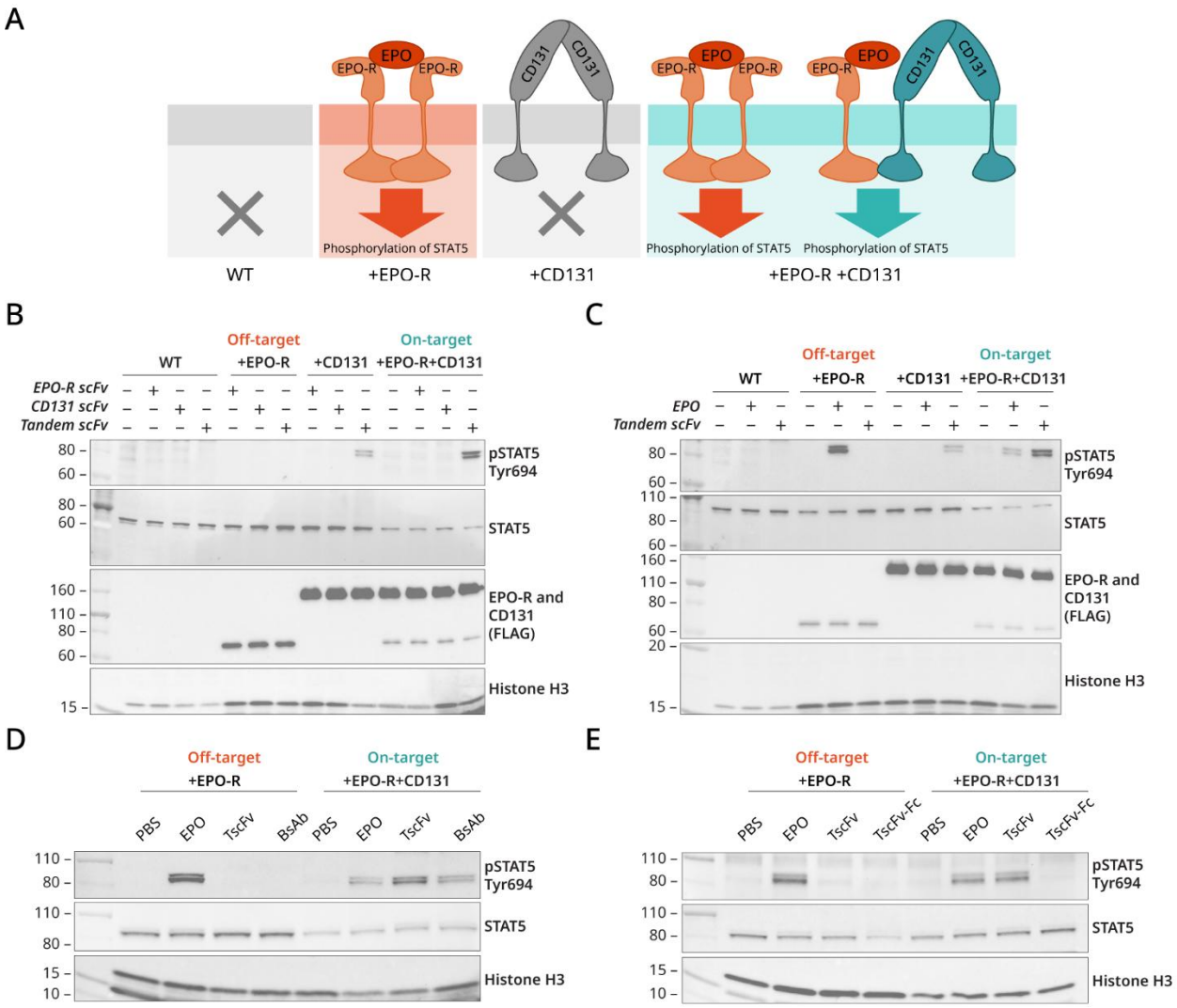

Figure 3. Tandem scFv and BsAb selectively activate STAT5 phosphorylation downstream of EPO-R/CD131 but not homodimeric EPO-R. A. Schematic of signaling in each overexpression line. HEK293T cells were stably transduced with FLAG-tagged expression constructs of either hEPO-R, hCD131, or both. Comparing the response between cells with both EPO-R and CD131 (which will have EPO-R/EPO-R and EPO-R/CD131 signaling) to cells with only EPO-R (which only can signal through EPO-R/EPO-R) can illuminate EPO-R/CD131-specific signaling. **B-E.** Cells were FBS starved overnight, treated with the designated proteins at 100nM for 15 min, and lysed in the presence of protease and phosphatase inhibitors. Proteins were run by SDS-PAGE and visualized by western blot with the designated antibodies. **B.** TscFv, but not the individual scFvs, triggers CD131-dependent STAT5 phosphorylation. **C.** TscFv has a different signaling profile than EPO and does not activate EPO-R/EPO-R. **D.** BsAb is also only able to induce STAT5 phosphorylation in cells that express CD131. **E.** TscFv-Fc does not activate STAT5 phosphorylation downstream of EPO-R/EPO-R nor EPO-R/CD131.

296 (**Figure 3A**). Additionally, unlike UT-7-ES1, HEK293T do not express the alpha subunit of
297 any CD131 receptor, so treatment response in these lines cannot be complicated by
298 activation of related CD131-containing receptors.

299 As expected, the anti-EPO-R and anti-CD131 monomeric scFvs did not induce STAT5
300 phosphorylation in any cell line (**Figure 3B**), most likely due to the inability of a monomeric
301 scFv to induce receptor dimerization. Also as expected, EPO induced STAT5
302 phosphorylation in both EPO-R and EPO-R/CD131 expressing cell lines (**Figure 3C**),
303 confirming functional EPO-R signaling in these lines. However, in contrast, TscFv induced
304 strong STAT5 phosphorylation only in cells that express both EPO-R and CD131, but not
305 the EPO-R-only cell line (**Figure 3B**). TscFv also induced weak STAT5 phosphorylation in the
306 CD131-only overexpression line (**Figure 3B**), which remains unexplained. To determine if
307 this effect was cell-line dependent, we separately constructed a HEK293T cell line
308 expressing a V5-tagged CD131 that expresses less CD131 (**Figure S3).** In this line, TscFv
309 did not induce detectable STAT5 phosphorylation (**Figure S4**). BsAb also induced STAT5
310 phosphorylation only when CD131 is expressed (**Figure 3D**).

311 To determine if simply the presence of both scFvs was sufficient for signaling, we
312 treated cells with an equimolar mix of the EPO-R and CD131 scFvs. An equimolar mix of
313 the scFvs did not induce STAT5 signaling in either the EPO-R only or EPO-R and CD131
314 overexpression cell lines (**Figure S5**), suggesting simultaneous binding and linking of both
315 receptors is necessary. Finally, consistent with the signaling and binding data, TscFv-Fc
316 was unable to activate STAT5 phosphorylation in either line at the same dose (**Figure 3E**).
317 In conclusion, TscFv and BsAb are most active in the EPO-R/CD131 cell line and not active
318 in cells expressing only EPO-R and that the bispecific nature of TscFv and BsAb is
319 necessary for activity. Therefore, induced proximity of EPO-R and CD131 by a single
320 bispecific molecule appears to be sufficient for receptor activation.

321

322 **Decreasing linker length between anti-EPO-R and anti-CD131 scFvs in TscFv modifies**
323 **signaling**

324 Based on the EPO-R/CD131/tandem scFv structural model **(Figure 1E)**, we
325 hypothesized that shortening the inter-scFv linker would reduce or eliminate downstream
326 signaling. Specifically, in our model, the C-terminus of the anti-EPO-R scFv and the N-
327 terminus of the anti-CD131 scFv are separated by 88 Å. The 23 aa linker in TscFv (denoted
328 GS-L, **Figure 4**) can cover this distance when fully extended. If this model is correct,
329 shortening the linker would likely reduce or eliminate signaling because the proper
330 geometry of EPO-R and CD131 would be entropically unfavored or sterically infeasible.

331 We designed several new TscFv variants with linkers of differing length and rigidity
332 (Chen *et al.*, 2013). Specifically, a tandem scFv with a 7-amino acid linker between the anti-
333 EPO-R scFv and the anti-CD131 scFv (SF for short, flexible); a tandem scFv with a 23-amino
334 acid rigid linker between the anti-EPO-R scFv and the anti-CD131 scFv (LR for long, rigid); a
335 tandem scFv with a 7-amino acid rigid linker between the anti-EPO-R scFv and the anti-
336 CD131 scFv (SR for short, rigid); and a tandem scFv with no linker (NL) (**Figure 4**). We also
337 rearranged the anti-EPO-R scFv so that its linker attachment point is further away from the
338 anti-CD131 scFv ("Swap") (**Figure 4)**.

339

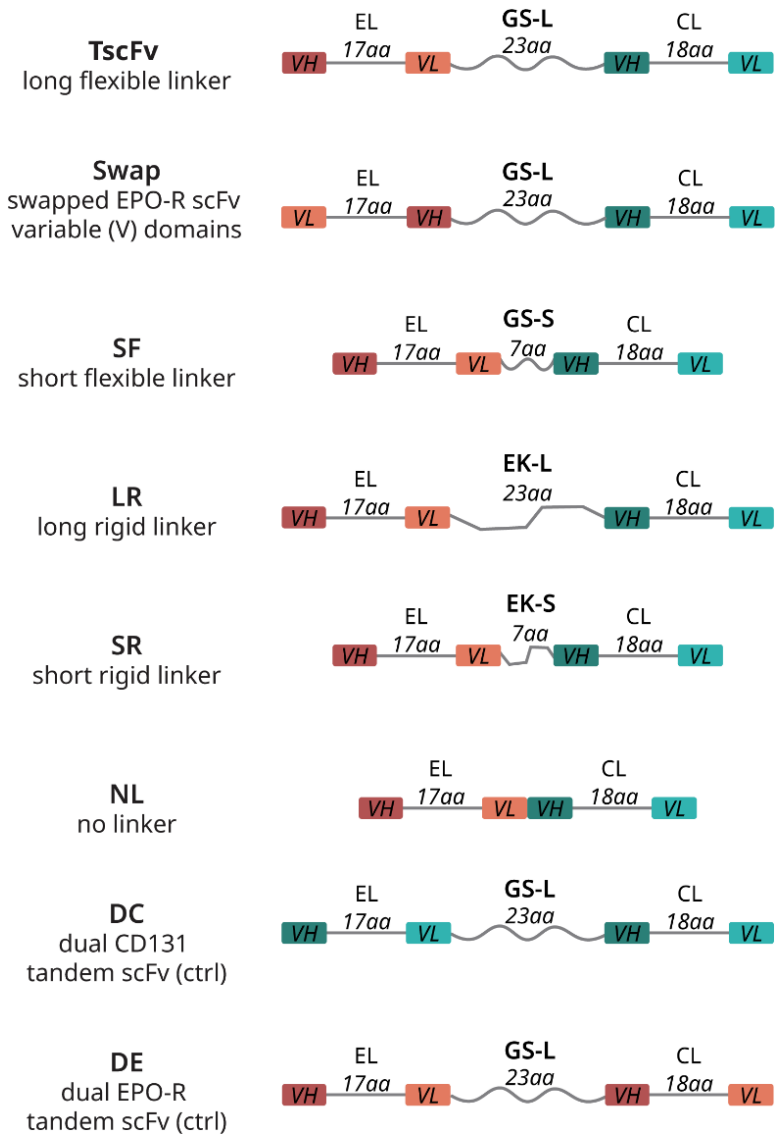

Linker	Sequence
EL	GGGGSGGGGSSGGGGSS
GS-L	GSGEGGSESSGEGSGESSGEGSG
CL	GSGGGSSSGGSGSSGGSG
GS-S	ESSGEGS
EK-L	EAAAKEAAAKEAAAKEAAAKEAA
EK-S	EAAAKEA

Figure 4. Design of tandem scFv linker and domain variants. A. Variants were made of TscFv with changes to the linker connecting the two scFvs or the variable (V) domain order of the EPO-R scFv. Two control tandem scFvs (TscFv-DE and TscFv-DC) were also constructed to ensure signaling was due to the bispecific binding of TscFv, not just the presence of two scFvs. The linkers connecting the variable domains of each scFv (EL and CL) were kept the same in all constructs. The sequence of each linker is listed. Abbreviations: VH=heavy chain, VL=light chain, GS=Glycine and serine linker, EK=Glutamic acid and lysine linker, L=long, S=short.

347 The linker variants with no linker, shorter linkers, or more rigid linkers (NL, SF, SR,
348 LR) induced two to four-fold less STAT5 phosphorylation in parental UT-7-ES1 compared to
349 the original TscFv (which has a long, flexible linker) (**Figure 5A, 5B).** STAT5 phosphorylation
350 in the UT-7-ES1 CD131 KO cell line was greatly reduced or completely eliminated for all of
351 the linker variants (except "Swap"), suggesting CD131 dependent signaling (**Figure 5C,**
352 **5D**). In the UT-7-ES1 CD131 KO line, the "Swap" tandem scFv induced more STAT5
353 phosphorylation in comparison to TscFv (**Figure 5C, 5D**). We believe this is due to the
354 linker length between the two scFvs, which may force dimerization of the anti-EPO-R scFv
355 and enable some level of homodimeric EPO-R signaling.

356 All linker variants also induced STAT5 phosphorylation in the HEK293T line that
357 expresses EPO-R and CD131 (**Figure 5E, 5F**). TscFv variants with longer linkers (TscFv, LR)
358 are more efficacious than those with shorter linkers, consistent with the UT-7-ES1 results.
359 We also designed two tandem scFv controls, DC (dual anti-CD131 scFv) and DE (dual anti-
360 EPO-R scFv)), which each consist of two of the same scFv connected by a long, flexible
361 linker (**Figure 4**). Since it has two EPO-R binding moieties, DE should signal through EPO-
362 R/EPO-R, while the dual anti-CD131 scFv (DC) should not. As expected, DE induced a level
363 of STAT5 phosphorylation that is similar to EPO, and DC did not induce strong STAT5
364 phosphorylation (**Figure 5E, 5F**). Comparison of the response induced by TscFv, DE, and
365 DC further suggests that the induced STAT5 phosphorylation is not due to the presence of
366 two linked scFvs but is specific to the presence of both EPO-R and CD131 binding moieties
367 in the same molecule (**Figure 5E, 5F**).

368 Finally, we tested the ability of the TscFv linker variants to support proliferation of
369 UT-7-ES1. The maximum response (E_{max}) of the variants varies markedly (**Figure 5G**). TscFv
370 variants with shorter linkers induced less proliferation compared to the original (**Figure**
371 **5G)**. As expected, DE supported cell proliferation since it can signal through homodimeric
372 EPO-R in the UT-7-ES1 CD131 KO cell line (**Figure S6**). All of the linker variants induced little
373 or no proliferation in the UT-7-ES1 CD131 KO cell line (**Figure 5H**). Altogether, these data
374 indicate that TscFv and its variants require CD131 to support UT-7-ES1 proliferation,

suggesting they are more selective for EPO-R/CD131 than natural EPO.

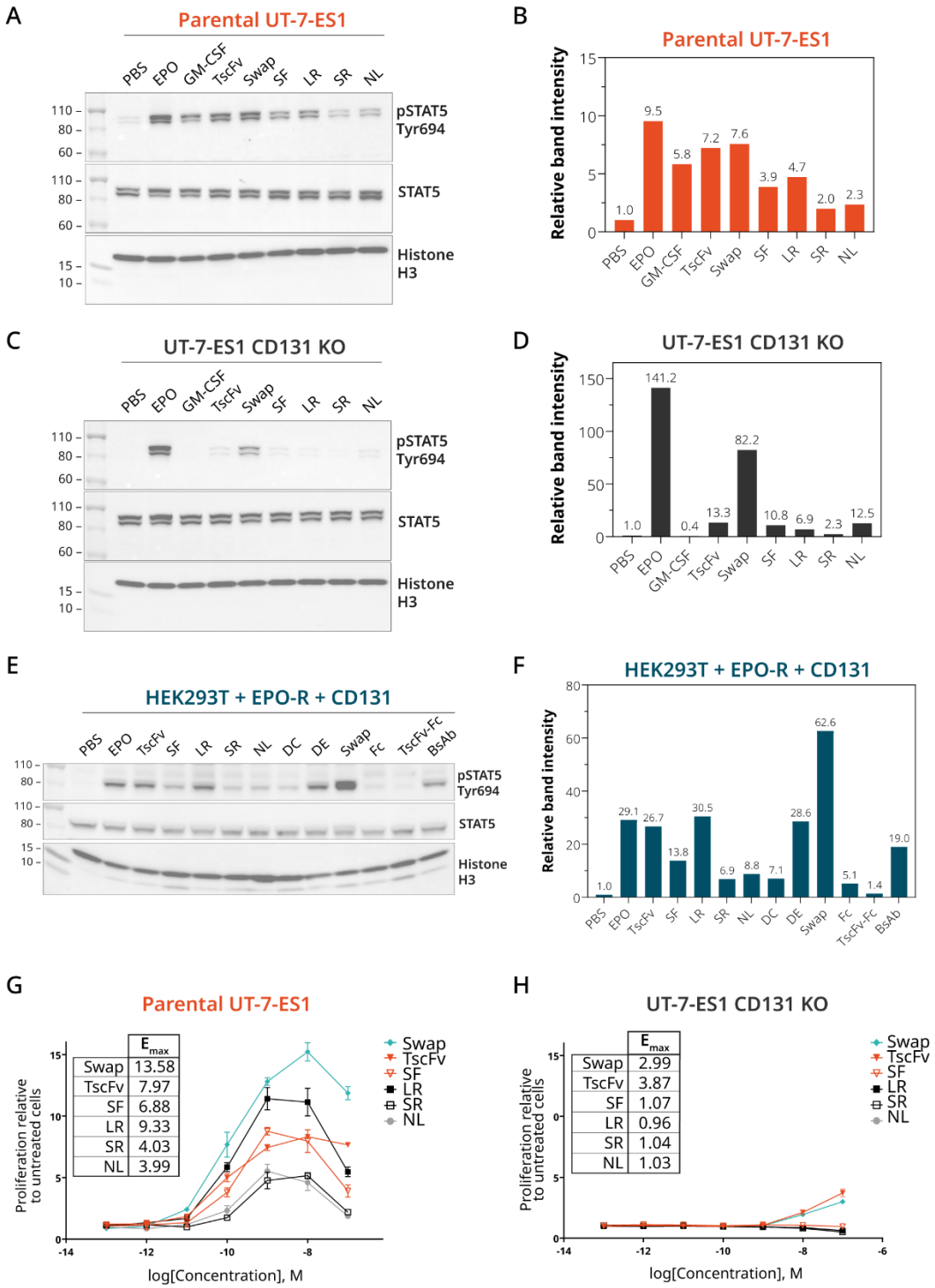

Figure 5. Decreased linker length between EPO-R and CD131 scFvs decreases signaling of tandem scFv variants. A, C. UT-7-ES1 or UT-7-ES1 CD131 KO cells were FBS starved overnight, treated with the designated

380 proteins at 100nM for 15 min, and lysed in the presence of protease and phosphatase inhibitors. Proteins were
381 run by SDS-PAGE and visualized by western blot with the designated antibodies. **B, D.** Band densities of STAT5
382 phosphorylated at Tyr694 in **A** and **C** were quantified and plotted relative to the density of the PBS-treated
383 control bands. **E.** HEK293T overexpressing EPO-R and CD131 were FBS starved overnight, treated with the
384 designated proteins at 100nM for 15 min, and lysed in the presence of protease and phosphatase inhibitors.
385 Proteins were run by SDS-PAGE and visualized by western blot with the designated antibodies. **F.** Band
386 densities of **E** relative to the PBS-treated control sample. **G.** TscFv and its variants are able to support UT-7-ES1
387 proliferation, but variants with decreased linker length induce less proliferation. Parental UT-7-ES1 lines were
388 cytokine starved overnight, treated with the designated proteins at 100nM and viability was measured 72 hrs
389 later. **H.** TscFv and linker variants are unable to support proliferation of UT-7-ES1 when CD131 is knocked out.
390 UT-7-ES1 CD131 KO cells were treated as in **G** and viability was measured 72 hrs later. Proliferation data are
391 reported as proliferation relative to untreated cells and are represented by mean luminescence ± SD of three
392 replicates. E_{max} values were calculated using GraphPad Prism.

393

394 ## Discussion

395 Signaling through a combination of EPO-R and CD131 is thought to promote
396 resistance to cell stress, such as neurons exposed to hypoxia or traumatic brain injury. In
397 this study, we developed selective EPO-R/CD131 agonists, based on joining anti-EPO-R and
398 anti-CD131 scFv modules. Previous work identified antibodies that bind to EPO-R (Lim *et*
399 *al.*, 2010; Moraga *et al.*, 2015) or CD131 (Panousis *et al.*, 2016) and solved the structure of
400 these scFvs in complex with their target antigen. We used AlphaFold 3 (Abramson *et al.*,
401 2024) to construct a model of an EPO-R/CD131 signaling complex, determined where V
402 regions from the anti-EPO-R and anti-CD131 antibodies would bind, and then designed
403 and expressed a tandem scFv (TscFv) consisting of an anti-EPO-R scFv, an anti-CD131 scFv,
404 and a linker long enough to connect them. Additionally, we constructed a bispecific
405 antibody (BsAb) by fusing the scFvs to a heterodimeric Fc. TscFv and BsAb induced STAT5
406 phosphorylation through activation of EPO-R/CD131, without engaging EPO-R/EPO-R
407 (**Figure 2, Figure 3**) and and also induced cell proliferation of UT-7-ES1 in a CD131-
408 dependent manner (**Figure 2, Figure 4)**. In addition, shortening the linker between the
409 scFvs reduced signaling in a manner consistent with the predicted structural model of

410 EPO-R/CD131. These proteins provide proof of concept for design of selective EPO-
411 R/CD131 agonists and lay a foundation for the development of a clinical-grade EPO-
412 R/CD131 biologic drug.

413 EPO and EPO variants can prevent cell death of non-hematopoietic cells in the face
414 of cytotoxic agents or hypoxia in *in vitro* and *in vivo* models of neurodegeneration and
415 trauma (Ghezzi and Brines, 2004; Grunfeld *et al.*, 2007; Patel *et al.*, 2012; Ponce *et al.*, 2013;
416 Noh *et al.*, 2014; Robinson *et al.*, 2018; Hemani *et al.*, 2021). However, the concentration
417 needed to generate this cell protective signaling (1-20 nM vs.100-200 pM for
418 hematopoietic effects) would lead to undesired effects, such as RBC and prothrombotic
419 platelet generation, due to activation of homodimeric EPO-R (Brines and Cerami, 2012).
420 Previous efforts to make specifically tissue-protective EPOs have centered around mutated
421 or modified EPO, such as carbamylated EPO or proteins with mutations in the face of EPO
422 that mediates the weak interaction with EPO-R (Leist *et al.*, 2004; Brines *et al.*, 2008; Gan *et*
423 *al.*, 2012; Pankratova *et al.*, 2012; Cho *et al.*, 2022). These molecules fortuitously happened
424 to have desirable properties, without a clear mechanism by which the EPO-R/CD131
425 signaling properties derive from the structure.

426 In this work, our strategy has been to construct molecules that bring EPO-R and
427 CD131 together via scFvs that bind to each receptor. The best selective EPO-R/CD131
428 activator is a single polypeptide chain tandem scFv consisting of an N-terminal scFv that
429 binds to EPO-R (Moraga *et al.*, 2015), a central 23-amino acid linker, and a C-terminal scFv
430 that binds to CD131 (Panousis *et al.*, 2016), denoted TscFv. The design of this molecule was
431 driven by a structurally plausible AlphaFold 3 model of interacting EPO-R and CD131.
432 However, the 23-amino acid linker has a maximum extended length of about 100
433 Angstroms, so the molecule could accommodate many possible configurations of EPO-R
434 and CD131.

435 TscFv stimulated the growth of UT-7-ES1 in a CD131-dependent manner and was
436 not active in cells that only express EPO-R (**Figure 2E, 2F, 5G, 5H**). This is in contrast to a

437 tandem scFv consisting of two anti-EPO-R scFvs (denoted DE; **Figure 4, S6**), which was not
438 impaired by loss of CD131. (These observations also suggest that TscFv assembles as
439 diagrammed, and does not form dimers in which two anti-EPO-R scFvs form a diabody
440 that could link two EPO-Rs). Specific signaling through EPO-R/CD131 was observed in two
441 paired cell lines: UT-7-ES1 parental cells compared to UT-7-ES1 CD131-knockout cells
442 (**Figure 2, 5**), and HEK293T cells engineered to express EPO-R only or both EPO-R and
443 CD131 (**Figure 3, 5**). When parental UT-7-ES1 cells were treated with TscFv, the level of
444 STAT5 phosphorylation was comparable to that induced by EPO, while in the UT-7-ES1
445 CD131 knockout cells, only a trace of STAT5 phosphorylation was observed. The UT-7-ES1
446 parental cells proliferated in response to TscFv and its variants (**Figure 4, 5G, 5H**), while
447 the UT-7-ES1 CD131 knockout cells did not proliferate at all in response to any of these
448 proteins (**Figure 2E, 2F, 5G, 5H**). Similarly, TscFv stimulated STAT5 phosphorylation in
449 HEK293T cells expressing both EPO-R and CD131, but not cells expressing only EPO-R
450 (**Figure 3**).

451 Based on our results, we envision that a practical therapeutic protein that
452 specifically activates EPO-R/CD131 complexes could be constructed. Such proteins could
453 be used to treat neurological disorders, such as traumatic brain injury (Robinson *et al.*,
454 2018), ALS (Noh *et al.*, 2014; Lauria *et al.*, 2015), and possibly also Alzheimer's disease
455 (Kalluru *et al.*, 2024). To be useful in these chronic conditions, such a molecule should not
456 induce autoantibodies to endogenous EPO and should have a long plasma half-life.
457 Repeated administration of EPO-based scaffolds introduces the risk of triggering an
458 autoimmune response to endogenous EPO (Casadevall *et al.*, 2005; Tamilvanan *et al.*,
459 2010). In contrast, our constructs will not induce autoantibody production to EPO as they
460 differ significantly in structure.

461 Pharmacokinetics represents a further challenge. Human EPO has a plasma half-
462 live of only a few hours, but nonetheless has been a successful drug since the major use of
463 EPO is to treat kidney failure patients who are on dialysis (Kalantar-Zadeh, 2017). Typically,

464 such patients undergo dialysis three times per week, and IV administration of EPO
465 through the line already set up for the dialysis is practical in this context. Moreover, in
466 treating anemia it is not essential to have continuous exposure to EPO, as long as there is
467 production of red blood cells, which have a lifetime of about 100 days. However, in
468 treating a neurodegenerative disorder, continuous EPO signaling may be necessary.
469 Boesch et al. (Boesch *et al.*, 2007, 2008) performed a pilot clinical trial on 12 patients with
470 Friedreich's ataxia and saw a favorable effect on biomarkers; the patients received EPO
471 three times per week, the same dose that a dialysis patient would receive, but a dose that
472 likely enhances thrombotic events due to induction of EPO-R/EPO-R signaling. In
473 subsequent trials of EPO and carbamylated EPO for Friedreich's ataxia, patients were
474 dosed once every two to three weeks (Mariotti *et al.*, 2012; Boesch *et al.*, 2014).
475 Additionally, Lauria et al. (Lauria *et al.*, 2015) clinically tested EPO as a treatment for ALS,
476 also dosing once per two weeks. Given EPO's plasma half-life in humans of about 8 hrs,
477 the patients' nervous systems would be unprotected for most of each dosing period. Our
478 anti-EPO-R/anti-CD131 tandem scFv has a much larger Stoke's radius than EPO and
479 carbamylated EPO, which should lead to a superior plasma half-life. Moreover, current
480 fusion protein technologies allow for profound extension of plasma half-life, such that
481 high levels of a protein drug can be maintained for several weeks. With this in mind, we
482 designed BsAb, which consists of the EPO-R and CD131 scFvs fused to Fc. BsAb is also
483 selective for EPO-R/CD131 and will likely have a superior plasma half-life due to its size and
484 Fc receptor (FcRn)-mediated recycling (Kontermann, 2011). However, before such
485 technologies can be applied successfully, it is necessary to have a structural
486 understanding of how the active protein element binds to its targets, as we have sought
487 to reveal in the present experiments.

488 In conclusion, we report the rational design of several bispecific selective protein
489 agonists of EPO-R/CD131. These fusion proteins serve as a foundation for future studies of
490 EPO-R/CD131 biology and the development of next-generation cytokine mimetics with
491 improved specificity and reduced off-target effects.

492 # Methods

493 ## DNA construct design and generation

494 The anti-EPO-R scFv sequence was obtained from Moraga et. al (Moraga *et al.*,
495 2015) (PDB 4y5y) and the anti-CD131 scFv sequence was obtained from Panousis et. al
496 (Panousis *et al.*, 2016) (PDB 5dwu). These sequences were codon-optimized and cloned
497 into pSecTag2a. An engineered heterodimeric fragment crystallizable (Fc) domain of
498 mouse IgG2a (H4A, H4B) (Wang *et al.*, 2019) was used in the Fc fusion constructs. The Fc
499 fusions were tagged with His6 on one monomer (H4B) to increase the likelihood of
500 purification of only heterodimeric proteins. All protein expression constructs included a
501 secretion signal to enable purification in mammalian cells. Sequences for the spacers of
502 the gRNAs for CD131 KO were designed using the Custom Alt-R™ CRISPR-Cas9 guide RNA
503 tool from IDT against the human CSFR2B locus. Complete sequences of human EPO-R and
504 human CD131 were taken from UniProtKB ID P19235 and UniProtKB ID P32927
505 respectively and human codon-optimized using Benchling.

506 Plasmids were constructed using multiple fragment isothermal assembly using
507 NEBuilder® HiFi DNA Assembly Master Mix (NEB E2621L) or were ordered as Twist clonal
508 genes. Protein expression plasmids were assembled into pSecTag2a or pOptivec (with
509 added secretion signal from the V-J2-C region of the mouse Ig kappa-chain) to enable
510 protein secretion into the media. All secreted proteins were His6-tagged to enable
511 purification. Overexpression constructs and CRISPR gene editing plasmids were
512 assembled into third-generation lentiviral plasmid backbones for packaging into lentivirus.
513 All plasmids were sequence-verified before use via whole plasmid long-read sequencing
514 (Plasmidsaurus). See Supporting Information for more information on each plasmid
515 (**Supplementary Table 1**), protein sequences (**Supplementary Table 6**), full plasmid
516 sequence files and more detailed information on cloning procedures.

517

518

519 **AlphaFold structural prediction**

520 The final predicted structure of the tandem scFv, hEPO-R and hCD131 (**Figure 1E**)
521 was constructed using a combination of AlphaFold 3 (Abramson *et al.*, 2024) and the
522 pyMOL align feature. PyMOL align in combination with AlphaFold was used as AlphaFold 3
523 predictions of the entire complex (tandem scFv/EPO-R/CD131) using the sequences alone
524 did not seem biologically plausible. In this model, the transmembrane domain of hEPO-R
525 was sticking perpendicular to the transmembrane domain of hCD131, and the structures
526 did not align well with the solved PDB structures (PDB: 4y5y and 5dwu) of each scFv bound
527 to its respective receptor. Instead, AlphaFold 3 sequences of the EPO-R scFv, hEPO-R and
528 two copies of hCD131 were input in AlphaFold 3 to generate a predicted structure. Then,
529 the same was done for the CD131 scFv, hEPO-R and two copies of hCD131. Using the
530 pyMOL align feature, these two structures were combined using the common elements of
531 hEPO-R and 2 hCD131 to align the structures. The model 0 structure was used in both
532 cases. This yields a predicted structure of the scFvs in complex with hEPO-R and two
533 copies of hCD131 (**Figure 1E**). The measurement feature in pyMOL was used to measure
534 the distance between the termini of the scFvs to design the tandem scFv linker and linker
535 variant proteins (**Figure 1, 4**). To ensure biological plausibility of the predicted complex,
536 the complex structure was overlaid on the solved structures of each scFv binding its
537 respective receptor from PDB (Moraga *et al.*, 2015; Panousis *et al.*, 2016) and examined for
538 alignment.
539

540 **Cell culture**

541 HEK293T (ATCC CRL-11268) were obtained from Dr. Rui Tong Quek (Harvard
542 Medical School) and cultured in DMEM (ATCC 30-2002) supplemented with 10% (v/v) fetal
543 bovine serum (FBS; Thermo 10082147). Stable HEK293T overexpression lines expressing
544 either hEPO-R, hCD131 or both hEPO-R and hCD131 were grown in HEK293T complete
545 media as described above supplemented with 10 µg/mL blasticidin (Thermo A1113903)
546 and/or 2.5 µg/mL puromycin (Thermo A1113803). FreeStyle 293-F cell lines (Thermo

547 R79007) were obtained from Dr. Timothy Chang (Harvard Medical School) and cultured in
548 FreeStyle 293 Expression Medium (Thermo 12338026) shaking at 130 rpm in sterile,
549 vented cap Erlenmeyer cell culture shaker flasks (Corning CLS431143-50EA or CLS431145-
550 25EA). UT-7 EPO S1 (UT-7-ES1) were obtained from Dr. R Rogers Yocum and were grown in
551 IMDM (no phenol red) (Thermo 21056023), 10% HI FBS (Thermo 10082147), 1X GlutaMAX™
552 Supplement (Thermo 35050079), and 20ng/mL human EPO (Peprotech 100-64). UT-7-ES1
553 with stable CD131 KO were cultured in complete UT-7-ES1 media supplemented with 10
554 µg/mL blasticidin (Thermo A1113903) and 2.5 µg/mL puromycin (Thermo A1113803).

555 HEK293T cell lines were passaged every 3-4 days by gently washing the cell
556 monolayer once with DPBS (Thermo 14190144) followed by lifting with TrypLE (Thermo
557 12605010) and reseeding at 1/10 – 1/20 dilution (~10% confluence). FreeStyle 293-F cells
558 and UT-7-ES1 cell lines were passaged every 3-4 days or when density reached 1 – 2 million
559 cells/mL and directly reseeded in new flasks at 0.3 – 0.5 million cells/mL. All cell lines were
560 maintained at 37°C and 5% CO_2 in a humidified incubator. A full list of cell lines generated
561 in this work and the corresponding figures they are used in is located in **Supplementary**
562 **Table 5**.

563

564 **Lentivirus and stable cell line generation**

565 Briefly, stable HEK293T cell lines expressing hEPO-R or hCD131 or both hEPO-R and
566 hCD131 and the UT-7-ES1 CD131 KO line were generated by lentiviral transduction
567 followed by selection with 10 µg/mL blasticidin (Thermo A1113903) and/or 2.5 µg/mL
568 puromycin (Thermo A1113803) depending on the construct. Cells were transduced,
569 incubated for 24-48 hrs and then changed into selection medium. Cell samples were
570 collected once cells recovered to >95% viability to analyze transgene expression or gene
571 KO via SDS-PAGE and western blot or sequencing. See the Supporting Information for
572 more details on the transduction procedure for each of these lines. A full list of cell lines

573 generated in this work and the corresponding figures they are used in is located in
574 **Supplementary Table 5**.

575

576 **SDS-PAGE and Immunostaining**

577 Protein samples or cell lysate were diluted in 4X Laemmli SDS sample buffer
578 (Thermo J60015.AD) and diH_2O water to yield a final 1X Laemmli concentration. Samples
579 were boiled at 95°C for 5 minutes to denature proteins and then loaded on 4 to 20% Tris-
580 Glycine gradient gels (Thermo XP04205BOX) submerged in 1X Tris-glycine running buffer
581 (Thermo LC2675). Between 100 ng and 10 µg total protein (depending on application)
582 were run alongside 5-10 µL of Novex™ Sharp Pre-stained Protein Standards (Thermo
583 LC5800) for 1 hr at 200V. Gels were rinsed once with diH_2O, stained using SimplyBlue™
584 SafeStain (Thermo LC6065) following the manufacturer's protocol, and imaged using the
585 Coomassie setting on a ChemiDoc MP (Bio-rad 12003154).

586 Gels for immunostaining were instead removed from the cassette, rinsed once with
587 diH_2O in a dish and transferred to a nitrocellulose membrane (Thermo IB23002) according
588 to the manufacturer’s protocol using the P0 setting on the iBlot 2 gel transfer device
589 (Invitrogen IB21001). Blots were washed twice while shaking in TBST (TBS (Thermo
590 J60877.K3) + 0.05% Tween-20 (Millipore Sigma P9416-50ML)) and blocked for 1 hr at room
591 temperature or overnight at 4°C while shaking in TBST + 1% BSA (GoldBio A-420-10).
592 Primary antibody was added directly to the blocking solution and incubated shaking for 1
593 hr at room temperature or overnight at 4°C. Residual primary antibody was removed by
594 washing three times in TBST. Blots were then incubated in secondary antibody diluted in
595 TBST + 1% BSA for 1 hr at room temperature or overnight at 4°C while shaking. Blots were
596 washed three times in TBST to remove unbound secondary antibody, and developed and
597 imaged using SuperSignal West Dura Extended Duration Substrate (Thermo Scientific
598 34075) and the Chemi setting on a ChemiDoc MP. To quantify western blot signal, band
599 intensities for phospho-STAT5, total STAT5, and the loading control (histone H3) were

600 measured using the ImageLab densitometry software. Bands were background corrected
601 individually by the software, and background-corrected intensities were normalized to the
602 loading control from the same well to account for variations in sample loading. The
603 corrected, normalized phospho-STAT5 signal was then normalized to the corresponding
604 STAT5 signal to account for differences in protein expression levels across samples.
605 Finally, all normalized values were expressed relative to the samples treated with the
606 negative control (PBS), which was set to 1. More detail about the immunostaining protocol
607 and full gel or blot images and analyses are provided in the Supporting Information.
608 Antibody catalog numbers and dilutions are listed in **Supplementary Table 3**.

609

610 **Protein expression and purification**

611 Proteins were expressed transiently in HEK293-F cells using 293-fectin (Thermo
612 12347019) following the manufacturer's protocol. Flasks were incubated for 4-6 days at
613 37°C, 5% CO2 and shaking at 130 rpm to allow expression and secretion of proteins into
614 the medium. Cells were pelleted and the cell supernatant containing the expressed
615 proteins was isolated. His-tagged proteins were purified from the cleared cell supernatant
616 using His60 Ni Superflow Resin and buffers (Takara 635677) following the manufacturer's
617 protocol. Fractions were taken at each step for later analysis by SDS-PAGE and western
618 blotting using anti-6X His-HRP antibody (Abcam ab1187). Eluted proteins were
619 concentrated and buffer exchanged into endotoxin-free PBS (TekNova P0300) using
620 Amicon Ultra-15 Centrifugal Filters (Millipore-Sigma UFC901008 or UFC901024 depending
621 on protein size) according to the manufacturer's protocol. Protein concentration was
622 assessed using a BCA Protein Assay Kit (Thermo 23227) following the manufacturer's
623 protocol. Purified, concentrated proteins were aliquoted, flash frozen in liquid nitrogen,
624 and stored at -80°C until use. Aliquots were not freeze-thawed more than once to protect
625 protein integrity. A list of all proteins generated in this study is located in **Supplementary**
626 **Table 4**.

627

628 **Cell lysate generation**

629 3-8 million HEK293T or HEK293T overexpression lines or 4 million UT-7-ES1/UT-7-
630 ES1 CD131 KO clone C cells were washed three times using 1X TBS (Thermo J60877.K3) to
631 remove excess cytokine and/or FBS and plated in 60mm dishes or 6-well dishes in serum
632 and cytokine starved media (DMEM only (ATCC 30-2002) for HEK293T lines; IMDM only
633 (Thermo 21056023) for UT-7-ES1). The next day, lysis buffer (1X RIPA (CST 9806S)
634 supplemented with protease and phosphatase inhibitors (Thermo A32961) was prepared
635 and chilled to 4^0C. Wash buffer was prepared and chilled to 4^0C by supplementing 1X TBS
636 with protease and phosphatase inhibitors. Proteins were diluted in media without serum
637 and cytokines to 1 μM, added to cells to yield a final in-plate concentration of 100 nM, and
638 incubated for exactly 15 minutes at 37^0C and 5% CO_2. Cells were washed in wash buffer
639 once and moved to 1.5mL tubes and pelleted by centrifugation for 2 min at 300xg. The cell
640 pellet was resuspended in 200 – 400 μL of lysis buffer and lysed according to the
641 manufacturer's protocol. Protein concentration of the lysates was taken by BCA. Lysates
642 were normalized to the same concentration before analysis by western blotting. See
643 Supporting Information methods for more details.

644

645 **UT-7-ES1 cell proliferation assays**

646 UT-7-ES1 or UT-7-ES1 CD131 KO clone C cell lines were washed three times using
647 TBS to remove residual cytokines and seeded in white, flat-bottom, clear 96-well plates
648 (Millipore Sigma CLS3610) at 9.0 x 10^3 cells per well in 90 μL of growth medium with no
649 growth factors (IMDM + 10% FBS only). The following day, purified proteins were serially
650 diluted 10-fold (10^{-6} M to 10^{-12} M) in growth medium with no growth factors in 96-well
651 plates (Corning 3641) and 10 μL of protein dilution or medium was added to the cells.
652 Plates were gently swirled and then incubated at 37°C in 5% CO2 for 72 h. Cell
653 proliferation was determined by Cell Titer Glo (Promega G7572) following the

654 manufacturer's protocol. Luminescence was read on a BioTek Synergy Neo HTS microplate
655 reader using the Luminescence fiber default protocol. Background (media only wells)
656 luminescence was subtracted from each sample and each well's corrected luminescence
657 was divided by the luminescence of untreated cells. Data are reported as proliferation
658 relative to untreated cells and are represented by mean luminescence ± SD of three
659 replicates. EC_{50} and E_{max} were calculated using GraphPad Prism using nonlinear regression
660 (log(agonist) vs. response, variable slope (four parameters).

661

662 **Enzyme-linked immunosorbent assay (Elisa)**

663 Recombinant human EPO-R (RND systems 963-ER) or human CD131 (AcroBio CD1-
664 H5256-100 µg) was diluted to 1 µg/mL in PBS and 50 µL per well was added to coat
665 MaxiSorp 96-well ELISA plates (Sigma M9410). Plates were incubated shaking overnight at
666 4°C and then washed five times in wash buffer (PBS + 0.05% Tween-20 (PBST) (Millipore
667 Sigma P9416-50ML)). Plates were blocked with 200 µL per well of blocking buffer (PBS +
668 3% BSA (GoldBio A-420-10)) for 2 hrs shaking at RT and then washed five times with PBST.
669 His-tagged proteins were serially diluted in PBS, 50 µL per well of each dilution was added,
670 and the plate was incubated for 3 hrs shaking at RT or overnight shaking at 4°C. Plates
671 were washed five times with PBST to remove unbound proteins. Detection antibody (anti-
672 His HRP (Abcam ab1187)) was diluted 1/10,000 in PBS + 3% BSA, and 50 µL was added to
673 each well and incubated at RT shaking for 1hr. Plates were washed five times with PBST to
674 remove unbound antibody. 100 µL of room temperature TMB Substrate solution (Thermo
675 34028) was added to each well and absorbance was monitored until A_{620} reached >0.8 OD.
676 2M sulfuric acid was added to stop the reaction, and absorbance was measured at 450
677 nm. Data are reported as mean A_{450} ± SD of three replicates. EC_{50} and E_{max} were calculated
678 using GraphPad Prism using nonlinear regression (log(agonist) vs. response, variable
679 slope (four parameters).

680

Acknowledgements

The authors thank Professor Timothy Mitchison who provided thoughtful advice on experimental direction. K.E.D. would like to thank Drs. Ethan Jones, Neil Dalvie, Rui Tong Quek, and Kasia Kready for their helpful comments on the manuscript. K.E.D would like to additionally acknowledge the Harvard Systems, Synthetic, and Quantitative Biology PhD program, the Harvard Therapeutics Graduate Program (TGP), and the FujiFilm Fellowship for funding and support.

Author Contributions

K.E.D designed the project direction, conceptualized, designed and performed the experiments, made the structural model, and analyzed the data. K.E.D and J.C.W. created the figures and wrote the manuscript. K.E.D., J.C.W, and P.A.S. edited and approve the manuscript.

Conflict of interests

The authors declare no competing interests.

Funding

This work was supported by funds from the Department of Defense's Congressionally Directed Medical Research Programs (CDMRP) (TP230429), the Henry Jackson Foundation (award 6615; Air Force Research Laboratory award FA8650-21-2-6250), and the Harvard Brain Science Initiative Seed Grant.

K.E.D., J.C.W., and P.A.S. were also supported by the Harvard Medical School Department of Systems Biology. K.E.D was additionally supported by the Systems,

Synthetic and Quantitative Biology PhD program (training award: T32GM135014), the Harvard Therapeutics Graduate Program (TGP) and the FujiFilm Fellowship (2021-2022).

Corresponding Authors

Jeffrey C. Way − Department of Systems Biology, Harvard Medical School, Boston, Massachusetts 02115, United States; Wyss Institute for Biologically Inspired Engineering, Harvard University, Boston, Massachusetts 02115, United States

Email: jeffrey_way@hms.harvard.edu

https://orcid.org/0000-0002-6676-3188

Authors

Kailyn E. Doiron − Department of Systems Biology, Harvard Medical School, Boston, Massachusetts 02115, United States; Wyss Institute for Biologically Inspired Engineering, Harvard University, Boston, Massachusetts 02115, United States

Email: kdoiron@fas.harvard.edu

Secondary Email: kailynd126@gmail.com

https://orcid.org/0000-0001-5208-788X

Pamela A. Silver − Department of Systems Biology, Harvard Medical School, Boston, Massachusetts 02115, United States; Wyss Institute for Biologically Inspired Engineering, Harvard University, Boston, Massachusetts 02115, United States

Email: pamela_silver@hms.harvard.edu

https://orcid.org/0000-0002-7856-4071

References

Abramson,J., Adler,J., Dunger,J., *et al.* (2024) *Nature*, **630**, 493–500.

Ainavarapu,S.R.K., Brujić,J., Huang,H.H., *et al.* (2006) *Biophys. J.*, **92**, 225.

Anagnostou,A., Lee,E.S., Kessimian,N., Levinson,R. and Steiner,M. (1990) *Proc. Natl. Acad. Sci. U. S. A.*, **87**, 5978–5982.

Boesch,S., Nachbauer,W., Mariotti,C., *et al.* (2014) *Mov. Disord.*, **29**, 935–939.

Boesch,S., Sturm,B., Hering,S., Goldenberg,H., Poewe,W. and Scheiber-Mojdehkar,B. (2007) *Ann. Neurol.*, **62**, 521–524.

Boesch,S., Sturm,B., Hering,S., Scheiber-Mojdehkar,B., Steinkellner,H., Goldenberg,H. and Poewe,W. (2008) *Mov. Disord.*, **23**, 1940–1944.

Borges,L.G., Ketchem,R.R., Lim,A.C., Mehlin,C. and Zhou,H. (2008) Erythropoietin receptor agonists.

Brines,M. and Cerami,A. (2008) *J. Intern. Med.*, **264**, 405–432.

Brines,M. and Cerami,A. (2012) *Mol. Med. Camb. Mass*, **18**, 486–496.

Brines,M., Grasso,G., Fiordaliso,F., *et al.* (2004) *Proc. Natl. Acad. Sci.*, **101**, 14907–14912.

Brines,M., Patel,N.S.A., Villa,P., *et al.* (2008) *Proc. Natl. Acad. Sci.*, **105**, 10925–10930.

Broudy,V.C., Lin,N., Brice,M., Nakamoto,B. and Papayannopoulou,T. (1991) *Blood*, **77**, 2583–2590.

Burrill,D.R., Vernet,A., Collins,J.J., Silver,P.A. and Way,J.C. (2016) *Proc. Natl. Acad. Sci.*, **113**, 5245–5250.

Carr,P.D., Gustin,S.E., Church,A.P., *et al.* (2001) *Cell*, **104**, 291–300.

Casadevall,N., Eckardt,K.U. and Rossert,J.A.A.C.A. (2005) *J. Am. Soc. Nephrol.*, **16**, S67.

Caveney,N.A., Rodriguez,G.E., Pollmann,C., *et al.* (2024) *Mol. Cell*, **84**, 1995-2005.e7.

Chen,X., Zaro,J. and Shen,W.C. (2013) *Adv. Drug Deliv. Rev.*, **65**, 1357–1369.

Cheung Tung Shing,K.S., Broughton,S.E., Nero,T.L., *et al.* (2018) *Sci. Rep.*, **8**, 12457.

Chin,H., Nakamura,N., Kamiyama,R., Miyasaka,N., Ihle,J.N. and Miura,O. (1996) *Blood*, **88**, 4415–4425.

757 Cho,B., Yoo,S.J., Kim,S.Y., Lee,C.H., Lee,Y.I., Lee,S.R. and Moon,C. (2022) *Redox Biol.*, **49**,
758 102223.

759 Ercan,I., Tufekci,K.U., Karaca,E., Genc,S. and Genc,K. (2018) In Donev,R. (ed), *Advances in*
760 *Protein Chemistry and Structural Biology*. Academic Press, pp. 309–357.

761 Gan,Y., Xing,J., Jing,Z., Stetler,R.A., Zhang,F., Luo,Y., Ji,X., Gao,Y. and Cao,G. (2012) *Stroke*,
762 **43**, 3071–3077.

763 Ghezzi,P. and Brines,M. (2004) *Cell Death Differ.*, **11 Suppl 1**, S37-44.

764 Grunfeld,J.F., Barhum,Y., Blondheim,N., Rabey,J.M., Melamed,E. and Offen,D. (2007) *Exp.*
765 *Neurol.*, **204**, 260–263.

766 Hanazono,Y., Sasaki,K., Nitta,H., Yazaki,Y. and Hirai,H. (1995) *Biochem. Biophys. Res.*
767 *Commun.*, **208**, 1060–1066.

768 Hansen,G., Hercus,T.R., McClure,B.J., *et al.* (2008) *Cell*, **134**, 496–507.

769 He,L., Cohen,E.B., Edwards,A.P.B., *et al.* (2019) *iScience*, **17**, 167–181.

770 Hemani,S., Lane,O., Agarwal,S., Yu,S.P. and Woodbury,A. (2021) *Neurochem. Res.*, **46**, 732–
771 739.

772 Hernández,C.C., Burgos,C.F., Gajardo,A.H., Silva-Grecchi,T., Gavilan,J., Toledo,J.R. and
773 Fuentealba,J. (2017) *Neural Regen. Res.*, **12**, 1381–1389.

774 Jubinsky,P.T., Krijanovski,O.I., Nathan,D.G., Tavernier,J. and Sieff,C.A. (1997) *Blood*, **90**,
775 1867–1873.

776 Kalantar-Zadeh,K. (2017) *Am. J. Nephrol.*, **45**, 235–247.

777 Kalluru,P.K.R., Bhavanthi,S., Vashist,S., Gopavaram,R.R., Mamilla,M., Sharma,S.,
778 Gundoji,C.R. and Goguri,S.R. (2024) *Ann. Med. Surg.*, **86**, 3608–3614.

779 Klingmüller,U., Bergelson,S., Hsiao,J.G. and Lodish,H.F. (1996) *Proc. Natl. Acad. Sci. U. S. A.*,
780 **93**, 8324–8328.

781 Komatsu,N., Yamamoto,M., Fujita,H., *et al.* (1993) *Blood*, **82**, 456–464.

782 Kontermann,R.E. (2011) *Curr. Opin. Biotechnol.*, **22**, 868–876.

783 Lauria,G., Bella,E.D., Antonini,G., *et al.* (2015) *J. Neurol. Neurosurg. Psychiatry*, **86**, 879–886.

784 Lee,J., Vernet,A., Gruber,N.G., Kready,K.M., Burrill,D.R., Way,J.C. and Silver,P.A. (2021)
785 *Protein Eng. Des. Sel.*, **34**, gzab025.

Lee,J., Vernet,A., Redfield,K., Lu,S., Ghiran,I.C., Way,J.C. and Silver,P.A. (2020) *ACS Synth. Biol.*, **9**, 191–197.

Leist,M., Ghezzi,P., Grasso,G., *et al.* (2004) *Science*, **305**, 239–242.

Lim,A.C., Ketchem,R.R., Borges,L., *et al.* (2010) *Biochemistry*, **49**, 3797–3804.

Lippi,G., Franchini,M. and Favaloro,E.J. (2010) *Semin. Thromb. Hemost.*, **36**, 537–549.

Livnah,O., Stura,E.A., Middleton,S.A., Johnson,D.L., Jolliffe,L.K. and Wilson,I.A. (1999) *Science*, **283**, 987–990.

Macdougall,IainC., Neubert,P., Coles,GeraldA., Roberts,DavidE., Dharmasena,A.D. and Williams,JohnD. (1989) *The Lancet*, **333**, 425–427.

Mariotti,C., Fancellu,R., Caldarazzo,S., *et al.* (2012) *Mov. Disord.*, **27**, 446–449.

Masuda,S., Nagao,M., Takahata,K., Konishi,Y., Gallyas,F., Tabira,T. and Sasaki,R. (1993) *J. Biol. Chem.*, **268**, 11208–11216.

Moraga,I., Wernig,G., Wilmes,S., *et al.* (2015) *Cell*, **160**, 1196–1208.

Noh,M.Y., Cho,K.A., Kim,H., Kim,S.M. and Kim,S.H. (2014) *Neurosci. Lett.*, **574**, 53–58.

Pankratova,S., Gu,B., Kiryushko,D., Korshunova,I., Køhler,L.B., Rathje,M., Bock,E. and Berezin,V. (2012) *J. Neurochem.*, **121**, 915–923.

Panousis,C., Dhagat,U., Edwards,K.M., *et al.* (2016) *mAbs*, **8**, 436–453.

Patel,N.S., Nandra,K.K. and Thiemermann,C. (2012) *Crit. Care*, **16**, 229.

Philo,J.S., Aoki,K.H., Arakawa,T., Narhi,L.O. and Wen,J. (1996) *Biochemistry*, **35**, 1681–1691.

Ponce,L.L., Navarro,J.C., Ahmed,O. and Robertson,C.S. (2013) *Pathophysiology*, **20**, 31–38.

Robinson,S., Winer,J.L., Chan,L.A.S., *et al.* (2018) *Front. Neurol.*, **9**.

Sautina,L., Sautin,Y., Beem,E., *et al.* (2010) *Blood*, **115**, 896–905.

Scott,C.L. and Begley,C.G. (1999) *Int. J. Biochem. Cell Biol.*, **31**, 1011–1015.

Sergio,C.M. and Rolando,C.A. (2022) *Exp. Brain Res.*, **240**, 1303–1315.

Shimomura,S., Komatsu,N., Frickhofen,N., Anderson,S., Kajigaya,S. and Young,N.S. (1992) *Blood*, **79**, 18–24.

Sosnick,T.R., Benjamin,D.C., Novotny,J., Seeger,P.A. and Trewhella,J. (1992) *Biochemistry*, **31**, 1779–1786.

Syed,R.S., Reid,S.W., Li,C., *et al.* (1998) *Nature*, **395**, 511–516.

Tamilvanan,S., Raja,N.L., Sa,B. and Basu,S.K. (2010) *J. Drug Target.*, **18**, 489–498.

Wang,F., Tsai,J.C., Davis,J.H., *et al.* (2019) *mAbs*, **12**, 1685350.

Watowich,S.S. (1999) *Int. J. Biochem. Cell Biol.*, **31**, 1075–1088.

Watowich,S.S. (2011) *J. Investig. Med. Off. Publ. Am. Fed. Clin. Res.*, **59**, 1067–1072.

Watowich,S.S., Hilton,D.J. and Lodish,H.F. (1994) *Mol. Cell. Biol.*, **14**, 3535–3549.

Watowich,S.S., Liu,K.D., Xie,X., Lai,S.Y., Mikami,A., Longmore,G.D. and Goldsmith,M.A. (1999) *J. Biol. Chem.*, **274**, 5415–5421.

Witthuhn,B.A., Quelle,F.W., Silvennoinen,O., Yi,T., Tang,B., Miura,O. and Ihle,J.N. (1993) *Cell*, **74**, 227–236.

Wojchowski,D.M., Gregory,R.C., Miller,C.P., Pandit,A.K. and Pircher,T.J. (1999) *Exp. Cell Res.*, **253**, 143–156.

Wrighton,N.C., Farrell,F.X., Chang,R., *et al.* (1996) *Science*, **273**, 458–464.